



Torsional behavior of GFRP-RC pontoon decks with an edge cutout and diagonal reinforcements

Xian Yang^a, Allan Manalo^{a,*}, Omar Alajarmeh^a, Brahim Benmokrane^b, Zahra Gharineiat^a, Shahradd Ebrahimzadeh^a, Charles-Dean Sorbello^c, Senarath Weerakoon^c

^a Centre for Future Materials (CFM), University of Southern Queensland, Toowoomba 4350, Australia

^b University of Sherbrooke, Department of Civil Engineering, Sherbrooke, Quebec, Canada

^c Boating Infrastructure Unit, Department of Transport and Main Roads, Brisbane City 4000, Australia

ARTICLE INFO

Keywords:

Torsional behavior
GFRP reinforced concrete deck
Edge cutout
Bar arrangements
Diagonal bars

ABSTRACT

Large-scale pontoon decks with edge cutouts were tested and the effect of diagonal reinforcements, arrangement of bars, and reinforcement-grid space size was investigated. The generated experimental data demonstrated the enhancement in the pre-cracking torsional behavior provided by diagonal reinforcement in double-layered reinforcement. Meanwhile, a further improvement in the reinforcement design with a denser grid spacing of 100 mm in double-layer mesh exhibited 137 % higher post-cracking torsional rigidity than that of the deck with a 250 mm grid spacing reinforcement. The former deck presented similar torsional behavior as the double-layered reinforced solid deck. The cracking torque and post-cracking torsional behavior of the pontoon decks can be accurately predicted with the introduced equations with consideration of the effective width related to the contribution of diagonal bars and considering the contribution of longitudinal GFRP bars, respectively.

1. Introduction

In maritime infrastructures elements, such as pontoon decks, torsional loading is normally caused by wave loading and/or by wave impact acting unevenly on different sides of the deck. If the deck is not designed properly, the twists result in inclined torsional cracks in the deck at a very early age, which allows moisture to penetrate and causes steel reinforcement to corrode. Fig. 1 presents the pontoon in wave action (from right side), torsional cracks and consequent reinforcement corrosion. Pursuing long-term endurance [1] and reduced maintenance costs, engineers are now interested in reinforcing pontoon decks with glass fiber-reinforced polymer (GFRP) bars. While the behavior of concrete structures reinforced with GFRP bars in flexure [2–6], shear [7,8], and compression [9,10] have been widely investigated, the understanding of their behavior under torsion is limited. Moreover, due to the inadequate experimental databases [11], most FRP-RC codes or design guidelines [12–14] in the world do not contain the provisions governing torsional design. Indeed, the Canadian Standards Association (CSA S806) standard [12] only covers the torsional design of beams. As

composite bars are now extensively used in concrete planks [4,15] and suspended flooring systems [16,17], there is a need to investigate their torsional behavior for effective and safe design.

Most of the reported works on torsional behavior have focused on steel-reinforced concrete beams. These studies have highlighted that the torsional strength and failure mechanism of RC structures under torsion are affected by concrete compressive strength, member geometry, depth-to-width ratio, concrete cover, and the relative amount of reinforcement in both directions [18–26]. Failure of beam under torsion manifest from brittle failure, ductile failure and clashing of concrete compressive struts depending on the amount of reinforcement [23,27]. Ibrahim et al. [21] found that the failure of the beams with thick concrete cover was controlled by concrete spalling and that the ultimate capacity of these beams was essentially equal to their initial crack. Some researchers experimentally compared the torsional behavior between steel reinforced beams and GFRP-RC beams [28,29]. Though GFRP-reinforced beams match steel's cracking torque and torsional strength, they exhibit larger deflections and cracks due to GFRP's lower Young's modulus. Unlike ductile steel, GFRP's brittleness requires

* Corresponding author.

E-mail addresses: xian.yang@usq.edu.au (X. Yang), allan.manalo@usq.edu.au (A. Manalo), omar.alajarmeh@usq.edu.au (O. Alajarmeh), brahim.benmokrane@usherbrooke.ca (B. Benmokrane), zahra.gharineiat@usq.edu.au (Z. Gharineiat), shahradd.ebrahimzadeh@usq.edu.au (S. Ebrahimzadeh), charles-dean.a.sorbello@msq.qld.gov.au (C.-D. Sorbello), senarath.Z.Weerakoon@msq.qld.gov.au (S. Weerakoon).

<https://doi.org/10.1016/j.istruc.2024.107438>

Received 26 September 2023; Received in revised form 11 August 2024; Accepted 28 September 2024

Available online 13 October 2024

2352-0124/© 2024 The Authors. Published by Elsevier Ltd on behalf of Institution of Structural Engineers. This is an open access article under the CC BY license (<http://creativecommons.org/licenses/by/4.0/>).



Fig. 1. Pontoon in wave action, torsional cracks and reinforcement corrosion.

careful assessment in torsional actions for GFRP-RC structures. Yang et al. [30] experimentally investigated the torsional performance of designed GFRP-RC decks and concluded that the post-cracking torsional rigidity of the tested decks was comparable to steel-reinforced isotropic concrete slabs [31] and beams fully reinforced with GFRP bars [32]. Given compelling evidence showcasing the benefits of higher GFRP reinforcement ratios in enhancing structural performance of GFRP-RC planks [4,7,15], it becomes imperative to investigate strategies for achieving enhanced torsional performance in GFRP-RC decks by strategically arranging the reinforcements.

As an edge cutout is a compulsory design in pontoon decks for pile accommodation purpose [33], Yang et al. [30] assessed the torsional behavior of GFRP-RC pontoon decks with edge cutouts and determined the edge cutout led to 17% lower cracking torque and 50% lower post-cracking torsional rigidity than those of the double layer reinforced solid decks. That is because the cutout reduced the torsional constant J in the deck's midspan and cut off some longitudinal reinforcement bars, making them not contributing to the torsional resistance. Other researchers observed the similar findings related to the negative effect of openings on the structural performance of slabs and beams [34–39]. Furthermore, they used FRP materials attached on the concrete surface or embedded in the concrete around the cutout for enhancement and achieved significant improvement in structural performance. The enhancement measure of embedded diagonal GFRP bars were selected herein and the actual performance of it under torsion should be practically investigated.

In summary, reinforced concrete (RC) pontoon decks are subjected to pure torsion caused by wave loading in marine environments, but the knowledge of their torsional behavior is limited. Moreover, edge cutouts negatively impact the structural performance of RC pontoon decks under torsion. Embedding diagonal GFRP bars could be a promising solution to mitigate this effect. This paper presents an experimental investigation of the torsional behavior of eight large-scale GFRP-RC pontoon decks. A design of diagonal reinforcement around the edge cutouts was proposed for enhancement. It was assessed together with other parameters: bar arrangement and grid space size on the failure mechanism, cracking torque, pre-cracking and post-cracking torsional rigidity, and post-cracking torsional strength. The applicability of ACI 318–14 (ACI 2014) provisions in predicting the cracking torque was evaluated by considering the effective width of the pontoon decks. Post-cracking torsional behavior was also predicted with a simple equation. The research findings and experimental datasets have contributed to a better understanding of the behavior of GFRP-RC pontoon decks subjected to torsion.

2. Experimental program

2.1. Materials

The pontoon decks tested in this study were reinforced with square-grid reinforcement mesh consisting of sand-coated high-modulus Grade III (#3) GFRP bars [40] (see Fig. 2(a)), with a nominal diameter of 10 mm. These bars were pultruded with unidirectional yarns of glass fibers impregnated with vinyl-ester resin, and their surface was sand-coated to enhance the bond strength with the surrounding concrete. These are the same GFRP bars used by Benmokrane et al. [41]; Table 1 provides their mechanical and physical properties. The concrete mix followed the provisions in MRTS70 [42], and the cast concrete was class S50 strength grade to meet the durability requirement for classification C2 in marine environments. The average concrete strength f_c obtained from the compression testing of concrete cylinders (see Fig. 2(b)) after 28 days is provided in Table 2 with the standard deviation in brackets. The pontoon design can benefit from deploying GFRP reinforcement by adapting the minimum 25 mm concrete cover for reinforcement protection, as suggested by Basaran and Kalkan [43], since this thickness has been found to not significantly affect the bond strength between the GFRP bars and concrete.

2.2. Specimen details

Pontoon decks reinforced with double layer of GFRP bars—with and without edge cutouts—were first designed. Afterwards, test parameters, including bar arrangement, grid space, and diagonal reinforcement, were applied in the design of the other specimens, as listed in Table 2. Dimension of the decks and reinforcement details were drawn in Fig. 3. It is noteworthy that the dimension of the edge cutout is selected by following Design Criteria for Floating Walkways and Pontoons [33]. As shown in Fig. 3, the first set of diagonal bars (650 mm long) were tied to the longitudinal bars at a 45° incline to the longitudinal axis and 25 mm offset from the edge cutout. The second set diagonal bars (850 mm long) were offset 100 mm from the first bars. The specimens were designated with a letter G—indicating sand-coated GFRP bars—followed by the reinforcement grid space in mm (150, 250, or 100); bar arrangement (L1 for single layered and L2 for double layered); geometry design/presence of diagonal reinforcement (S for solid, C for cutout without diagonal bars, D for cutout with single diagonal bars, DD for cutout with double diagonal bars); and T for torsion. For example, G100L2DDT is a deck with an edge cutout and is reinforced with a double layer of 100 mm square grid GFRP mesh and double diagonal reinforcement bars around the edge cutout in each layer of mesh. Decks G250L2CT, G150L1ST, and G250L2ST were set as references to evaluate the effect of diagonal bars, bar arrangement, and grid space, respectively.

2.3. Test setup and instrumentation

The pure torsion test was conducted in the mechanical test laboratory of the Centre for Future Materials at the University of Southern Queensland. The applied test setup was adapted with modifications from the test setup used by Derkowski and Surma [45]. Fig. 4 presents the photo of actual test setup in the laboratory. The specimen was totally fixed in the passive end by the passive support while the active end of the deck was free to spin around the pivot just below the deck. The center-to-center distance from active support to passive support was 2 m. More details about the supports were presented in the authors' previous publication [30]. Wave action is simplified as a torque applied at the ends of the decks which was generated by applying a load perpendicular to the spread beam using a 500 kN electrohydraulic jack with a 500 mm eccentricity. The load was applied in a displacement-control mode in a rate of 30 mm/min. A spherical hinge connected the load cell with the loading foot, ensuring the load foot was constantly perpendicularly pressing the spread beam of active end.



(a) Sand-coated GFRP bar (b) Compression test.

Fig. 2. GFRP bar and concrete cylinder compression test.

Table 1
Physical and mechanical properties of the GFRP bars [30,41].

Properties of #3 GFRP bar	Test method	Values
Nominal bar diameter (mm)	CSA S807 [12]	10
Nominal bar area (mm ²)	CSA S807 [12]	71
Ultimate tensile strength, f_u (MPa)	ASTM D7205/ D7205M–21 [44]	1315
Modulus of elasticity, E_{GFRP} (GPa)	ASTM D7205/ D7205M–21 [44]	62.5
Ultimate strain, ϵ_u (%)	ASTM D7205/ D7205M–21 [44]	2.3
Shear modulus, G_{grfp} (GPa)	[30]	1.37

Table 2
Test matrix.

Identifier	Ave f_c (MPa)	Grid space (mm)	Bar arrangement	Geometry	Diagonal reinforcement
G150L1DDT	76.8(6.4)	150	Single layer	Cutout	Double bars
G250L2DDT		250	Double layer	Cutout	Double bars
G100L2DDT		100	Double layer	Cutout	Double bars
G150L1DT		150	Single layer	Cutout	Single bar
G250L2DT		250	Double layer	Cutout	Single bar
G150L1ST		150	Single layer	Solid	N/A
G250L2ST		250	Double layer	Solid	N/A
G250L2CT		250	Double layer	Cutout	No

Displacement of the load point was recorded by the linear variable displacement transducer (LVDT) and a laser displacement sensor (LDS), as noted in Fig. 4. The LDS data was latter used to verify the LVDT data. Strains in the longitudinal and diagonal bars, as well as concrete were measured with 6 mm long electrical resistance strain gauges at the locations marked green in Fig. 3. During the test, a digital-image correlation (DIC) system was used to monitor deflection of the decks over the length of the loaded side by tracing the trajectories of the cross-marks drawn on the monitored surface in a 2D coordinate system. Only vertical deflections were collected for further analysis as the movement in other directions caused by concrete distortion were too small to be considered. Tests were stopped until cracks about 6 to 10 mm wide occurred in the concrete deck or until the deflection at the load point approached the maximum stroke of 85 mm.

3. Results and observation

3.1. Crack propagation

Fig. 5 shows the crack propagation in the GFRP-reinforced concrete deck along with the increase in torsional load and the crack pattern generated at the edge cutout at the end of the test. The initial cracks (marked in red) in most decks with edge cutouts—with the exception of G250L2DT—initiated from the corner of the edge cutout and extended toward the passive end at an inclined angle relative to the longitudinal axis, as shown in Fig. 5(a, b, c d, and h). For solid decks, the first crack appeared near the active end at loads of 64.7 kN (G150L1ST) and 66.1 kN (G250L2ST), the highest among all decks. Conversely, G250L2CT had the lowest cracking strength of 54.4 kN due to the narrowed mid-span width, as was explained by Yang et al. [30]. Decks with diagonal reinforcement around the edge cutout (e.g., G150L1DDT, G250L2DDT) exhibited higher cracking strengths, with G250L2DDT and G100L2DDT reaching 64.5 kN and 61.8 kN, respectively, nearly matching the solid decks. This indicates the positive impact of diagonal reinforcement on enhancing crack resistance at the edge cutouts.

Following initial cracks, additional torsional cracks formed near the deck edges at inclined angles, with existing cracks widening. Similar crack patterns appeared on the bottom surface, mirrored about the transvers midline. Marti et al. [46] reported the similar observations in steel-reinforced concrete slabs under torsion, although with denser crack spacing due to higher transverse reinforcement. In the decks with an edge cutout, cracks concentrated along the cutouts due to induced stress, promoting further cracking, as indicated in many studies [36,37, 39]. Notably, the edge cutout developed a significant horizontal shear crack toward the deck center (see Fig. 5. a, b, c, d, e, and h). The diagonal reinforcement design aimed to control torsional and shear cracks around the edge cutout area.

Fig. 6 provides video captures of cracking propagation at torsional loads of 70, 90, and 110 kN in the eight tested decks. The loads were selected because all specimens reached their within the post-cracking stage. Comparing G250L2DT to G250L2CT revealed that the single diagonal bar could restrain the shear crack at 70 kN, slightly above the concrete cracking strength. However, at 90 kN, both decks exhibited similar crack widths, indicating limited effectiveness of a single diagonal bar in the post-cracking stage. In contrast, double diagonal bars in deck G250L2DDT effectively restricted shear crack width throughout the test (see Fig. 6, c). Similarly, G150L1DDT, with double diagonal bars, avoided the wide torsional cracks seen in G150L1DT. Double diagonal bars enhanced crack control by increasing the contact surface with the

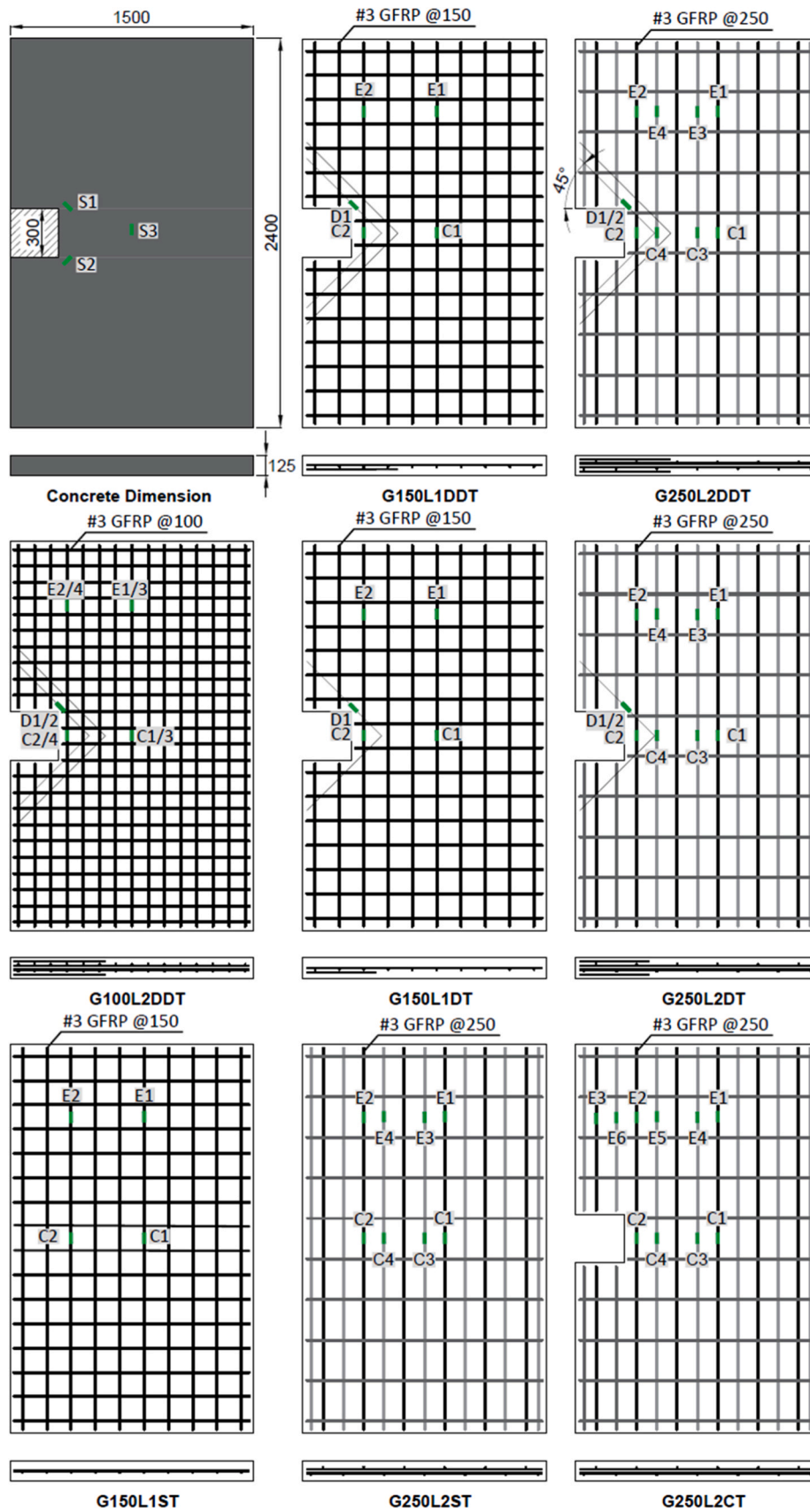


Fig. 3. Design details of tested decks.

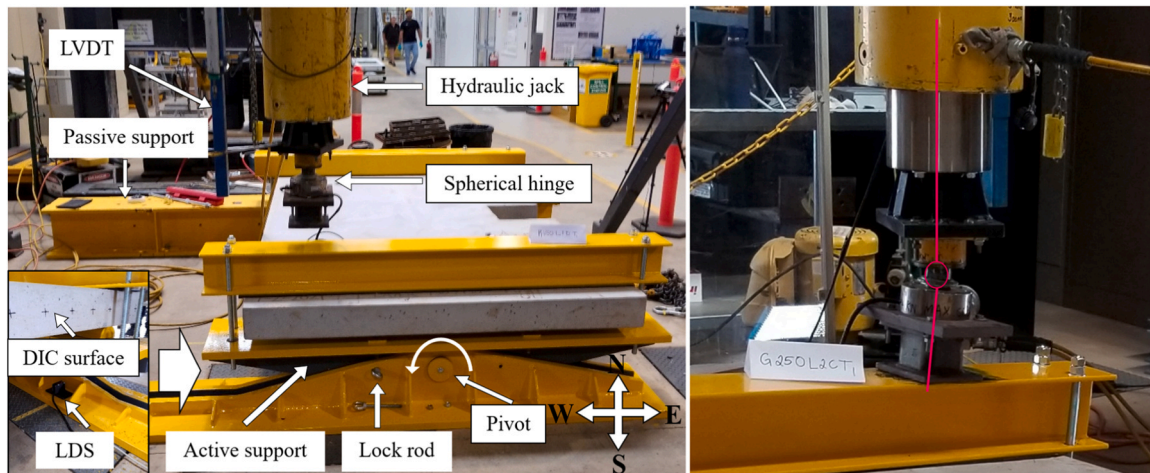


Fig. 4. Details of setup and close-in post-test photo.

concrete, impeding crack opening. Despite this, crack openings widened rapidly after initial cracks, as diagonal bars covered a small deck area and didn't significantly enhance torsional rigidity. Most decks with cutouts, except G100L2DDT, failed due to wide shear cracks. For example, G250L2CT nearly separated due to a horizontal shear crack at the cutout corner. The diagonal bars did not change the failure mode, but they delayed the crack widening.

In solid decks, G150L1ST failed due to significant torsional crack width and deformation, indicating serviceability loss. Conversely, the most densely reinforced deck, G100L2DDT, showed minimal shear crack width and length, highlighting the effectiveness of a dense grid space (100 mm) and double diagonal bars in restraining crack growth and minimizing twist deformation. No failures were observed in G250L2ST and G100L2DDT; only minor cracks appeared, with torsional force steadily increasing. Yang et al. [30] noted similar crack propagation in solid decks and RC beams reinforced with longitudinal GFRP bars and spaced GFRP stirrups under torsion, where failure was slow and gradual [28]. Furthermore, the research explained that the double meshes protected the concrete core from serious splitting and provided extra torsional resistance. The decks with a cutout failed similarly to GFRP-RC beams with only longitudinal reinforcement: concrete splitting failure [32].

3.2. Deflection measurements along the length of decks

The deflection measurements recorded using the DIC along the length of the tested decks at the first cracking load, 70 kN, 90 kN, 110 kN and the maximum applied load are presented in Fig. 7. The initial deflection curves showed a nearly linear trend, indicating the linear elastic behavior of the concrete. After the first crack, deflections increased significantly with minor load changes. Shear cracks appeared on the monitored side, causing a rapid increase in the deflection curve's gradient (α), indicating local stiffness degradation. For example, G150L1DDT (Fig. 7. (a)) showed gradient changes at 89.3 kN at 250 mm and 850 mm from the passive end, coinciding with shear crack locations demonstrated in Fig. 7(j). Ultimately, all the decks resulted in nonlinear profiles as the cracks made the decks discontinuous concrete media linked by the GFRP bars.

The deflection curves helped determine the crack width by measuring changes in gradient $|\Delta \tan \alpha|$ between three adjacent points, positively correlating with shear-crack width. At 70 kN, G150L1DDT's widest crack occurred at 1550 mm from the passive end with $|\Delta \tan \alpha|$ of 0.025, while G150L1DT had a similar crack with a maximum $|\Delta \tan \alpha|$ of 0.026 at 1450 mm. G250L2DDT had a maximum $|\Delta \tan \alpha|$ of 0.019 at 1950 mm, and G250L2DT had about 0.013 at 1050 mm. Accordingly, double-layered decks with diagonal bars, G250L2DDT and G250L2DT,

exhibited narrower shear cracks than their single-layered counterparts on the continuous side. Manalo et al. [4] observed similar results in GFRP-reinforced boat-ramp planks, noting narrower shear cracks in double-layered planks. At a higher load of 90 kN, G250L2DT exhibited a crack ($|\Delta \tan \alpha| = 0.030$ at 1050 mm) similar to that in double diagonal bars reinforced G250L2DDT ($|\Delta \tan \alpha| = 0.032$ at 750 mm). These crack widths were nearly half of the cracks generated in G250L2CT, in which the maximum $|\Delta \tan \alpha|$ was 0.024 at 70 kN and 0.056 at 90 kN, both at 2050 mm. This means that the diagonal bars on the discontinuous side not only limited crack expansion near the cutout but also affected crack growth on the continuous side. The findings indicate that double-layer reinforcement provides better crack control and structural integrity under torsional loads.

In the single-layered reinforced solid deck G150L1ST, crack widening reached a maximum $|\Delta \tan \alpha|$ of 0.060 at a maximum load of 126.5 kN. The most densely reinforced specimen (G100L2DDT) and the double-layered reinforced solid deck (G250L2ST) exhibited the narrowest shear cracks on the continuous side. At 70 kN, both G100L2DDT and G250L2ST had a maximum $|\Delta \tan \alpha|$ of 0.005, demonstrating the effectiveness of the dense reinforcement in controlling cracks. Moreover, at 110 kN, G100L2DDT had a crack width with $|\Delta \tan \alpha|$ of 0.019 at 1350 mm, while G250L2ST had a crack width with $|\Delta \tan \alpha|$ of 0.041 at 850 mm. G100L2DDT's crack growth on the continuous side was the slowest among all the tested decks. The design involving double-layered mesh, dense grid spacing, and double diagonal reinforcement bars enabled decks with edge cutouts to achieve crack control comparable to solid decks. Wide shear cracks indicate local stiffness degradation; therefore, an effective design can mitigate this degradation caused by concrete cracking.

3.3. Torque–twist response

Fig. 8 shows the torque–twist response of the pontoon decks tested under pure torsion. The general torsional behavior curves of the GFRP-RC decks are similar to the GFRP-RC beams tested by Deifalla et al. [29], Mohamed and Benmokrane [32], Hadhood et al. [47]. The torsion test was stopped between 0.07 rad/m and 0.09 rad/m, as significantly wide cracks (around 6 to 10 mm in width) were observed within this range. The fluctuation in the pre-cracking torque–twist curves (Fig. 8. (a)) caused by the vibration movement of the test machine loading head was quite obvious when the applied torque was over 20 kN·m and approaching the cracking torque. Therefore, the experimental pre-cracking torsional rigidity $(GJ)_{cr(exp)}$ was taken by regression equation for the initial part of the curves before 20 kN·m. The general slope of the curve between the first crack torque and maximum torque was used to estimate the experimental post-cracking torsional rigidity

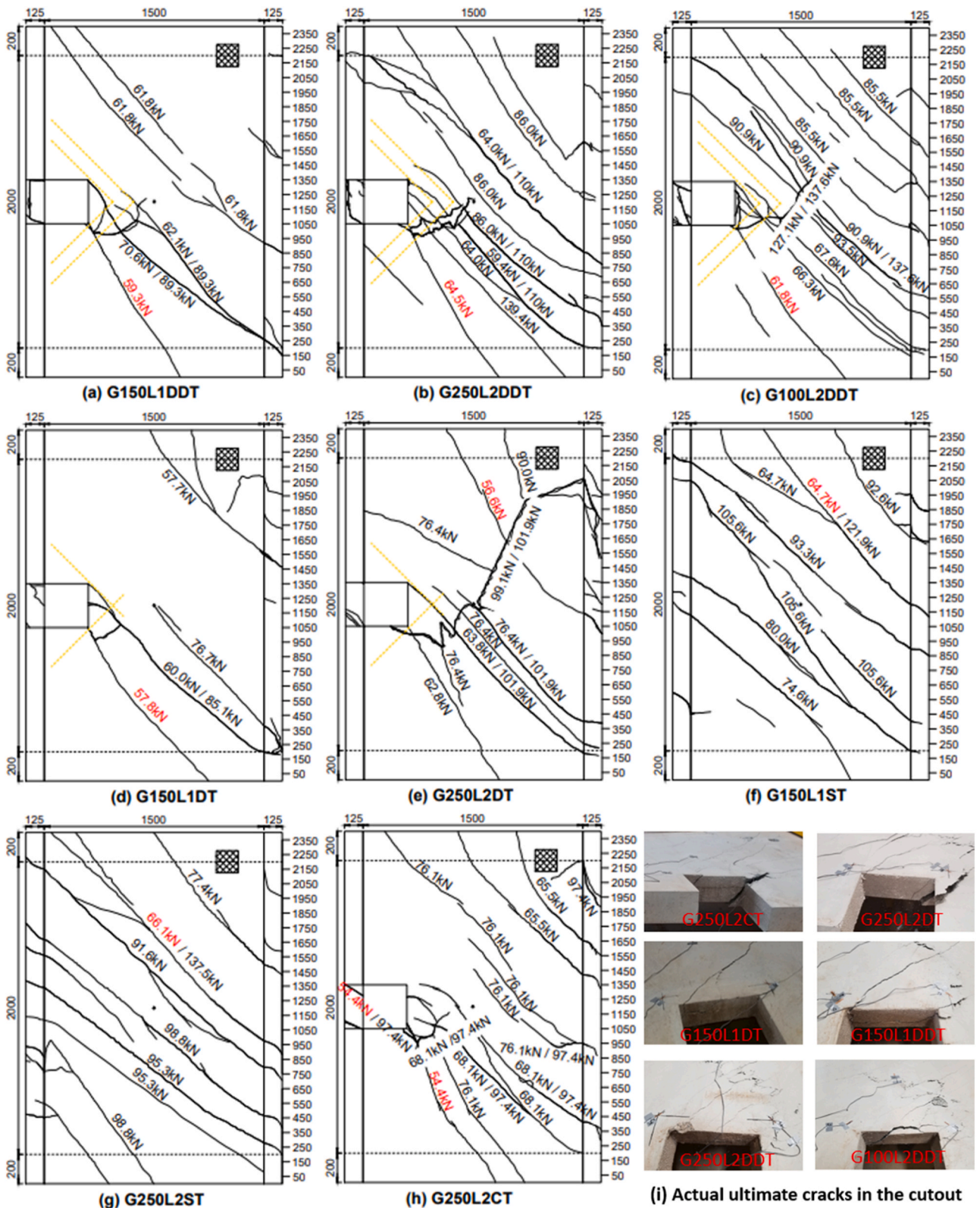


Fig. 5. Crack propagation schematic diagram and actual photos.

like that of the previous works [30–32]. The torsional rigidity decreased by about 95 % to 98 % after cracking occurred, indicating that most of the concrete was damaged at this point and would not be able to resist any applied torsion. The rigidity reduction after cracking was more significant when compared to that of the L-shaped GFRP-reinforced concrete beams tested by Deifalla et al. [29] (about 56 % to 73 %

reduction). That is probably due to the different dimensions of the structure and enclosed stirrups in the beams. Table 3 presents all the test results. The post-cracking torque strength at $\varphi = 0.07$ rad/m, —i.e., $T_{\varphi=0.07}$ in each specimen—was selected as the two single-layered reinforced decks (G150L1DT and G150L1DDT) only reached this level when the test was stopped.

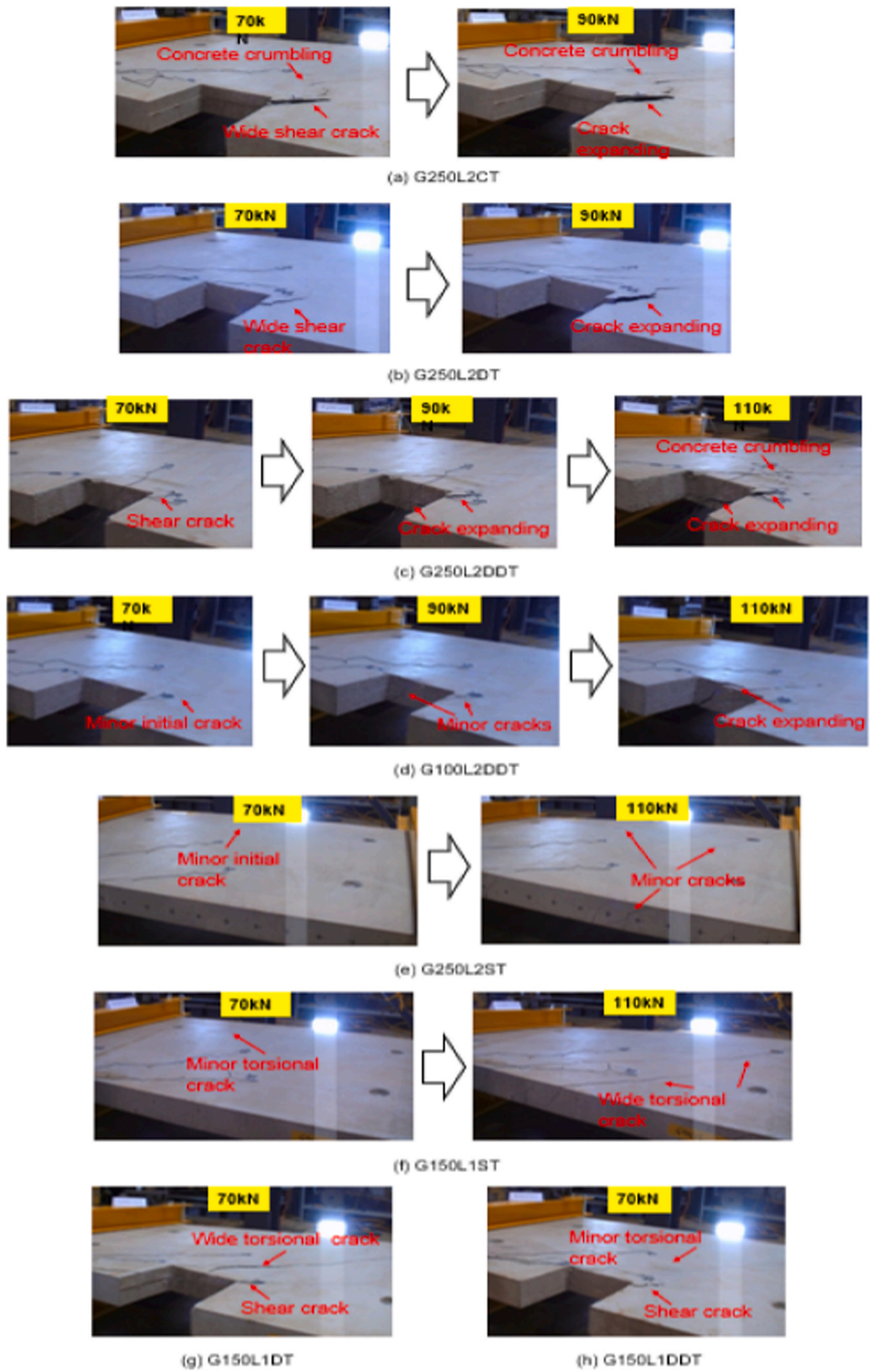


Fig. 6. Comparison of cracks at 70, 90, and 110 kN.

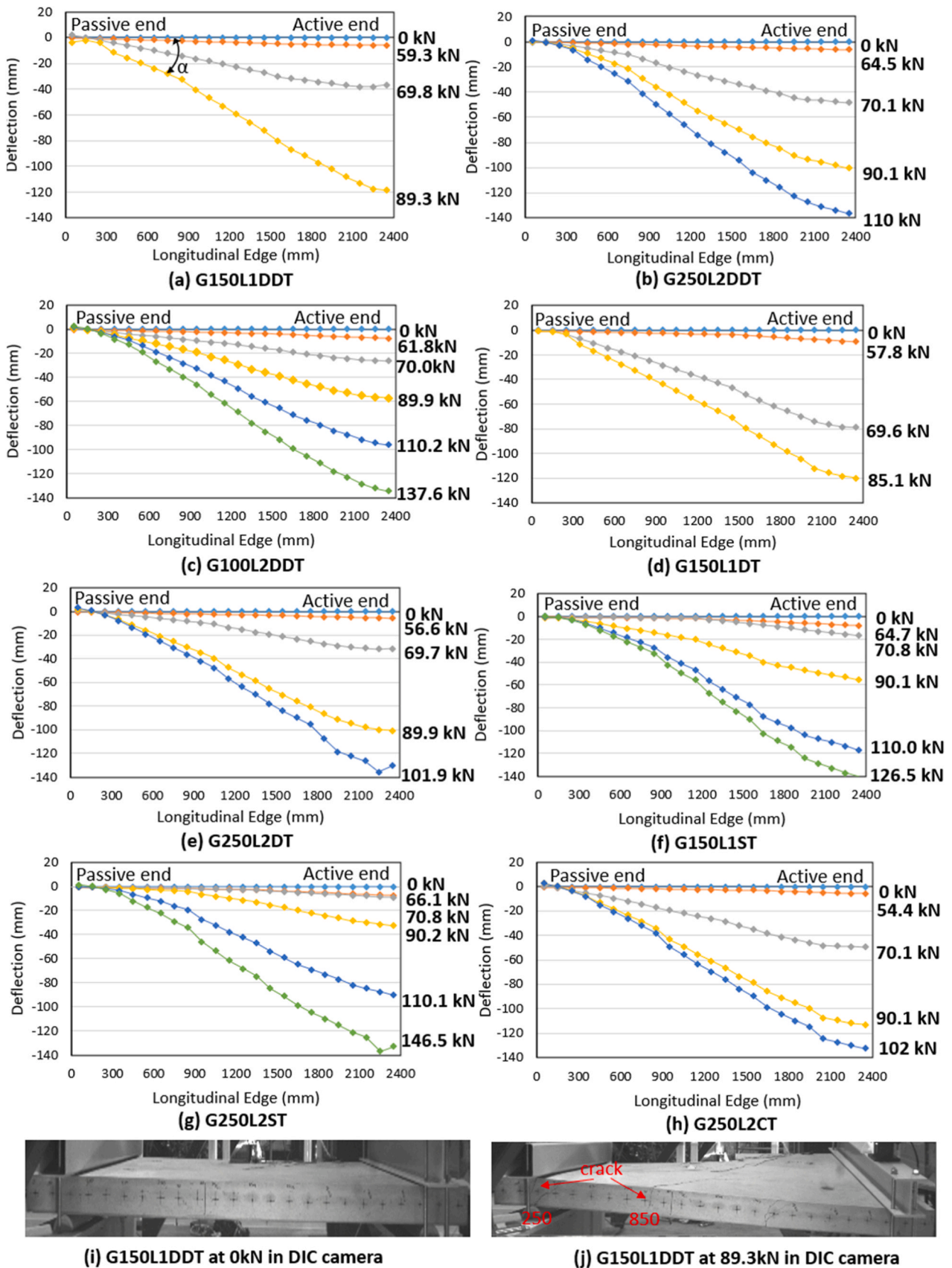


Fig. 7. Deflection along the length measured using the DIC.

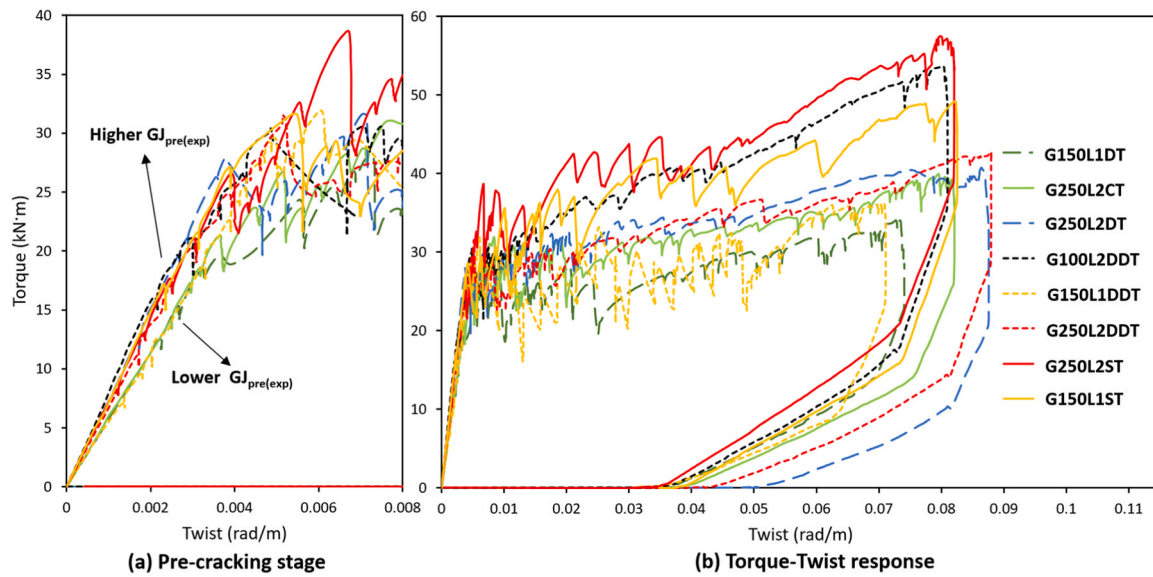


Fig. 8. Torque–twist response.

Table 3
Experimental results and prediction.

Specimen	$T_{cr} (exp)$ (kN·m)	$T_{cr} (pre)$ (kN·m)	ϕ_{cr} (rad/m)	ϕ_{max} (rad/m)	$(GJ)_{cr} (exp)$ (kN·m ²)	$(GJ)_{post} (exp)$ (kN·m ²)	$(GJ)_{post} (pre)$ (kN·m)	$T_{\phi=0.07} (exp)$ (kN·m)	$T_{\phi=0.07} (pre)$ (kN·m)
G150L1DDT	29.26	31.30 (+7.0 %)	0.0047	0.0750	5490	97	110 (+13.4 %)	35.72	31.30
G250L2DDT	31.54	31.30 (−0.8 %)	0.0051	0.0860	6339	130	153 (+17.7 %)	38.05	31.30
G100L2DDT	30.41	31.30 (+2.8 %)	0.0049	0.0803	7043	308	332 (+7.8 %)	50.50	54.54
G150L1DT	28.27	31.30 (+10.7 %)	0.0072	0.0734	5394	87	110 (+26.4 %)	32.15	31.30
G250L2DT	27.96	31.30 (+11.9 %)	0.0038	0.0752	7093	175	153 (−12.6 %)	39.82	31.30
G150L1ST	31.56	31.30 (−0.8 %)	0.0055	0.0823	6544	230	181 (−21.3 %)	46.87	31.30
G250L2ST	32.59	31.30 (−4.0 %)	0.0055	0.0800	6746	334	263 (−21.2 %)	53.57	49.71
G250L2CT	26.76	24.57 (−8.2 %)	0.0053	0.0796	5623	177	153 (−13.6 %)	37.15	24.76

3.4. Torque–strain behavior

Strain data were registered by the strain gauges marked green in Fig. 3. The strain gauge labels followed the rule as S for concrete surface, C for central reinforcement, E for edge reinforcement, and D for diagonal reinforcement. Unfortunately, some of gauges were damaged during concrete curing and did not record strains useful for analysis. The available strain data were analyzed and discussed as follows to better understand the mechanism of the tested GFRP-RC decks' behavior under torsion.

3.4.1. Torque–strain behavior on concrete

The torque–strain curves in Fig. 9 reveal that both tension and compression occurred on the concrete's top surface during torsion. Initially, strain gauges S1 (in compression) and S2 (in tension) recorded nearly equal strain levels near the cutout corner, indicating uniform torque distribution across the deck. The linear torque–strain response of S1 and S2 at the beginning reflects the concrete's linear elasticity. However, after reaching the cracking torque, the strain readings of S1 and S2 became erratic or were lost due to cracking and crumbling of concrete. Only S1 on G250L2DDT maintained a maximum compression strain of approximately $-1273 \mu\epsilon$ until maximum torsional force. The strain in the center area was minimal until the torque approached

maximum where S3 recorded high compression stress, indicating deck folding along its centroid under excessive twist deformation. For instance, G250L2DT generated extensive compressive cracking in the middle, traversing all tensile cracks before the test ended (Referring to Fig. 5e).

The initial response to strain varied among the decks. In decks without diagonal bars (G150L1ST, G250L2ST, and G250L2CT), the longitudinal bars near the first crack react first, confirmed by strain gauges E1, E4, and C2, due to stress transfer from concrete to reinforcement. In G250L2CT, the edge cutout corners induced stress concentration, evident from the lowest slopes in the S1 and S2 curves. In decks with diagonal bars, D1 strain gauge responded simultaneously with S1 and S2, indicating that diagonal bars shared the concentrated stress with the concrete. Strains values in S1 for G250L2DT, 250L2DDT and G100L2DDT were -64 , -101 , and $-85 \mu\epsilon$ at 20 kN·m, while D1 strains were -30 , -35 , and $-32 \mu\epsilon$ respectively, much lower than $-123 \mu\epsilon$ of S1 and $135 \mu\epsilon$ of S2 in G250L2CT under the same torque. The low strain values in S2 in three decks (80, 92, and $90 \mu\epsilon$ at 20 kN·m, respectively) also indicated that diagonal bars shared tensile stress, delaying the first crack occurrence by sharing stress at the cutout corner.

Strain gauge D2 in double-layered decks showed no strain before cracking, whereas D1 in single-layered decks showed slight tension. Fig. 10 illustrates stress distribution pre-cracking along the diagonal bar

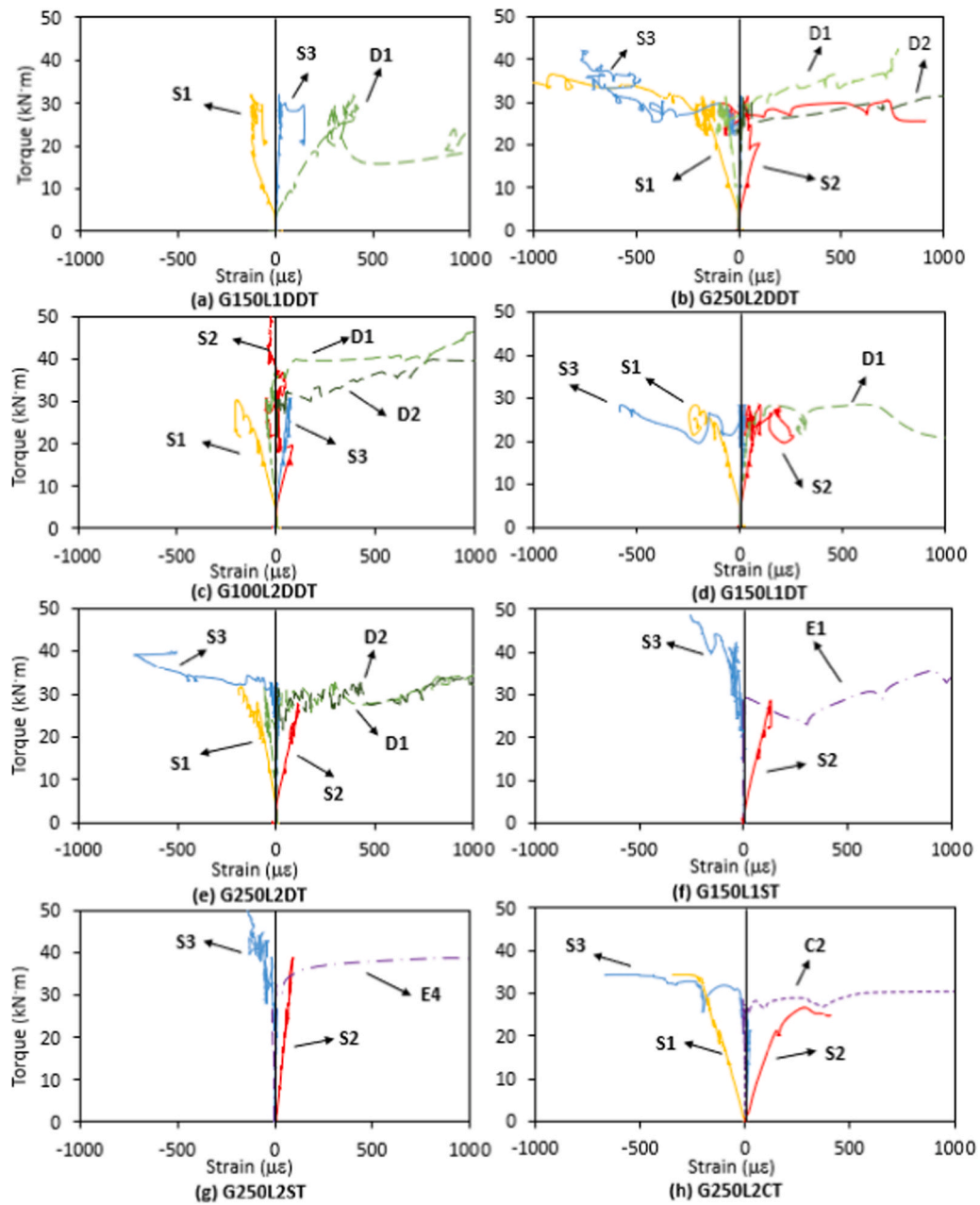


Fig. 9. Strain on the concrete surface and the GFRP bars first to react.

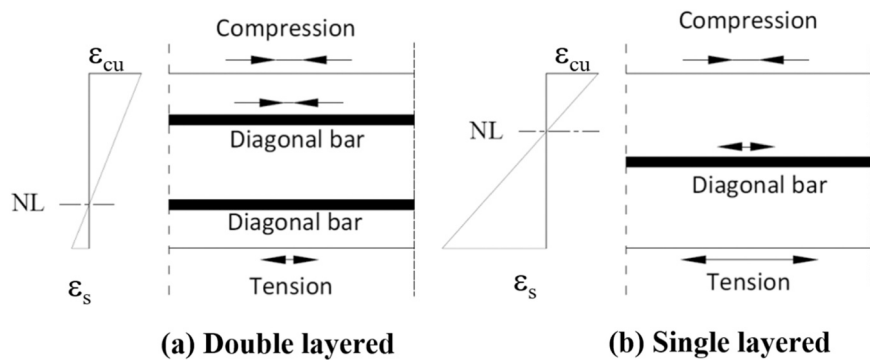


Fig. 10. Cross section profile along diagonal bar under G1.

under S1, based on recorded strains. The neutral line (NL) in double-layered decks was lower than in single-layered decks, with 80 % of concrete in compression versus less than 50 %. The arrangement of reinforcement in double-layered decks made better use of the concrete, making reinforcement more effective in resisting torsional forces in the pre-cracking stage.

3.4.2. Torque–strain behavior in the longitudinal bars

The torque–strain behavior in the longitudinal bars in each tested decks was plot in Fig. 11. Initially, there was no significant strain response in the bars until the cracking torque was reached, after which strain increased rapidly, indicating low post-cracking torsional resistance. The strain curves fluctuated due to the effect of concrete softening and reinforcement stiffening, as well as loading head vibration. Damaged strain gauges caused loops at the end of the curves (e.g., C3 on G250L2DDT, Fig. 11 (b)). The GFRP bars did not exceed their ultimate strain, indicating no bar damage at maximum torque. According to CSA S806–12 [12], the maximum allowable stress in GFRP bars embedded in reinforced concrete beams under torsion should not exceed $0.4 F_u$ or 1200 MPa, which equates to a maximum allowable strain of $9600 \mu\epsilon$ herein. As shown in Fig. 11, only C3 in G250L2DT and C2 in G250L2CT attached on the longitudinal bars in the central area, recorded strains near the maximum allowable strain shortly after cracking torque was reached (9392 and 12793 $\mu\epsilon$, respectively). Other decks (G250L2DDT, G150L1DDT, and G150L1DT) with similar or weaker post-cracking torsional rigidity might be in the same situation although some central area strain gauges were lost during specimen fabrication and handling. The high central area strain in these decks could be attributed to the concentrated stress induced by the edge cutout. In contrast, solid decks showed even stress distribution as central and end strain readings were almost the same.

In G100L2DDT, the highest strain occurred at C3 in the middle of the bottom layer reinforcement mesh. Comparing maximum strains at 33 kN·m for G250L2DT, G250L2DDT, and G100L2DDT, G100L2DDT's C3 strain was the lowest (2037 $\mu\epsilon$), while G250L2DDT and G250L2DT recorded C3 strains of 4824 and 5949 $\mu\epsilon$, respectively. Single diagonal bars resulted in 23.3 % higher strain than double diagonal bars in double-layered reinforced decks. G100L2DDT's C3 strain was only 42.2 % of G250L2DDT's C3 strain, due to denser reinforcement providing higher post-cracking torsional rigidity and less deformation under the same level of torque. C3 strain data is unavailable for G250L2CT, but C2 recorded a high strain of 12812 $\mu\epsilon$ at maximum torque of around 37 kN·m, significantly higher than any other double-layered decks with diagonal bars. This indicates the effectiveness of diagonal bars in reducing stress in critical reinforcement parts. The maximum strain in G250L2ST was 5323 $\mu\epsilon$ at 53.57 kN·m (E3), while in G100L2DDT it was 6618 $\mu\epsilon$ at 50.50 kN·m (C3), suggesting G100L2DDT's ultimate torsional capacity might be weaker than G250L2ST. Overall, denser grid space and double diagonal bars in double-layer reinforcement arrangements reduce critical stress induced by edge cutouts in post-cracking torsional behavior.

4. Discussion

4.1. Effect on initial cracking torque

The double-layered mesh combined with the diagonal bars increased the cracking torque despite the negative effect of edge cutout. The impact of bar arrangement on torsional cracking torque was negligible as shown in Table 3 that the three single-layered reinforced decks—G150L1DDT, G150L1DT, and G150L1ST—all generated similar levels of cracking torque compared to their double-layered reinforced counterparts with only 7.2 %, –1.1 %, and 3.2 % difference. Hsu [19] stated that torsional cracking is primarily influenced by the structure's aspect ratio and material properties. Thus, the variation of up to 7.2 % is likely due to the difference in concrete compressive strength.

Additionally, the most densely reinforced deck with a 100 mm grid space (G100L2DDT) and G250L2DDT with a 250 mm grid space had similar cracking torques. Due to the edge cutout, G250L2CT1 resulted in a lower torsional cracking torque (26.76 kN·m) compared to G150L1ST or G250L2ST (18.0 % or 21.8 % lower, respectively). Note that the edge cutout reduced the cross-sectional area of the concrete by 20 %. The employed diagonal bars improved the cracking torque performance by 9.3 % in G150L1DDT, 17.9 % in G250L2DDT, 13.7 % in G100L2DDT, 5.6 % in G150L1DT, and 4.5 % in G250L2DT when compared to G250L2CT. This was attributed to the strain measurement and analysis that revealed the diagonal bars near the edge cutout corner effectively distributed the concentrated stress, thus delaying the onset of cracking. The double-layered reinforced decks with double diagonal bars (G250L2DDT and G100L2DDT) had a larger increase in the cracking torque (up to 17.9 %), which was no surprise as the diagonal bars in the double-layered mesh were closer to the top and bottom concrete surface for an early response, and the double bars spread in the cracking direction had more contact surfaces with the concrete to share more stress than the single bars did.

4.2. Effect on pre-cracking torsional rigidities

Theoretical torsional rigidity GJ is mainly influenced by the torsional constant J , a function of cross section dimension, while G is the shear modulus of concrete. The presence of a cutout reduced $(GJ)_{pre(exp)}$ 18.2 % lower, on average, as demonstrated by G150L1ST (6544 kN·m²), G250L2ST (6746 kN·m²), and G250L2CT (5623 kN·m²). Similar to G250L2CT, the single-layered mesh reinforced decks with cutouts, G150L1DT and G150L1DDT, generated close $(GJ)_{post(exp)}$ values of 5394 and 5490 kN·m², respectively. On the other hand, the three double-layered reinforced decks with diagonal bars—G250L2DDT, G100L2DDT, and G250L2DT—had $(GJ)_{pre(exp)}$ values equal to or higher than the two solid decks (12.7 %, 25.3 % and 26.1 %, respectively). The double-layered reinforcement arrangement plus diagonal bars improved pre-cracking torsional rigidity, mitigating the negative effect of the edge cutout. That is due to the vertically distributed diagonal bars in the double meshes, which enhanced the weakest points at the cutout corners. Since no other reinforcement bars reacted to strains before cracking, only the diagonal reinforcement beside the edge cutout was considered to contribute to the pre-cracking torsional rigidity. Thus, it was concluded that the arrangement and spacing of reinforcement bars, in the absence of diagonal bars, did not have a significant effect on pre-cracking torsional rigidity.

4.3. Effect on post-cracking torsional rigidities

GFRP reinforcement was found to be the main factor affecting post-cracking torsional rigidity of the pontoon decks. Diagonal bars did not have a clear impact on post-cracking torsional rigidity as $(GJ)_{post(exp)}$ in decks G250L2CT and G250L2DT were almost identical. Single-layered reinforced decks with single set and double sets of diagonal bars showed only a 10.3 % difference in $(GJ)_{post(exp)}$, which was also close to a similar deck but without diagonal bars reported by Yang et al. [30]. The diagonal bars only helped bridge local shear cracks and did not contribute to the torsional rigidity after concrete cracking. Double-layered reinforced decks showed much higher $(GJ)_{post(exp)}$ compared to single-layered decks. G250L2DDT had a 33.6 % higher $(GJ)_{post(exp)}$ than G150L1DDT, and G250L2DT had double the $(GJ)_{post(exp)}$ of G150L1DT. The higher torsional rigidity in double-layered reinforced decks was due to the separated double-layered bar arrangement creating a higher J from GFRP mesh. The $(GJ)_{post(exp)}$ in G150L1DDT, G250L2DDT, G150L1DT, G250L2DT, and G250L2CT all generated at least 50 % lower $(GJ)_{post(exp)}$ than their solid-geometry counterparts due to the cut off discontinuous longitudinal bars. However, G100L2DDT had a $(GJ)_{post(exp)}$ only 7.7 % lower than the strongest double-layered reinforced solid deck (G250L2ST), which implies that

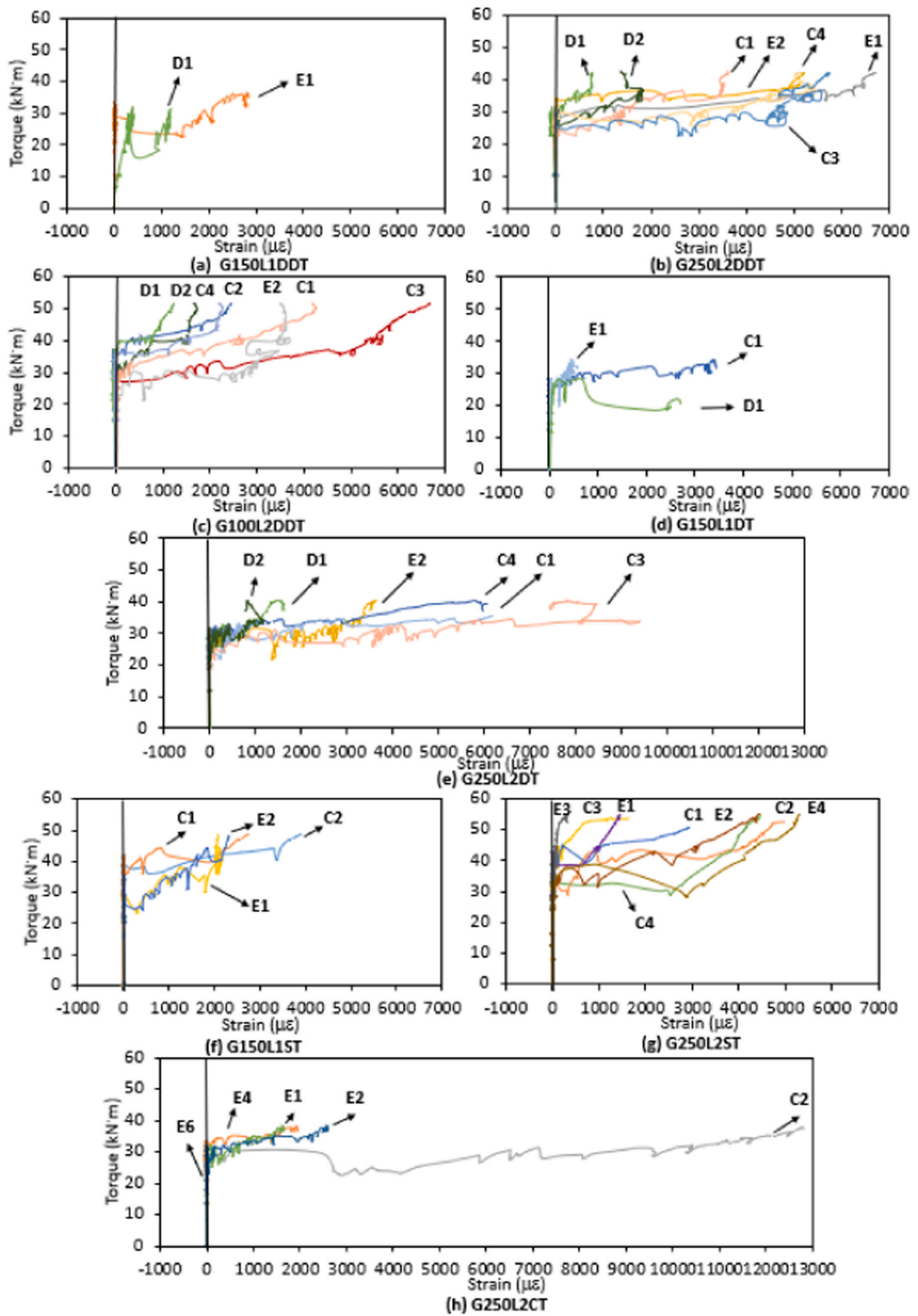


Fig. 11. Torque-strain behavior in the longitudinal bars.

the dense reinforcement design allowed a deck with an edge cutout to achieve comparable post-cracking torsional rigidities as a double-layered reinforced solid deck. That is because G100L2DDT had 2.4 times the number of continuous longitudinal bars resisting the torsion force than the three double-layered reinforced decks with an edge cutout. In general, the double-layered bar arrangement and denser grid space provided up to 137 % higher post-cracking torsional rigidities among double-layered reinforced decks, while the diagonal bars did not change the post-cracking torsional rigidity.

4.4. Effect on the post-cracking torsional strength

Large twist deformation for pontoon decks normally comes together with wide crack width, which should be avoided to maintain deck serviceability. So the post-cracking torsional strength at a limited twist of 0.07 rad/m, $T_{\varphi=0.07(\text{exp})}$, is discussed herein. The increases in torsional strength resulting from the use of GFRP mesh were 22.1 % in G150L1DDT, 20.6 % in G250L2DDT, 66.0 % in G100L2DDT, 13.8 % in G150L1DT, 42.4 % in G250L2DT, 48.5 % in G150L1ST, 64.4 % in G250L2ST, and 38.8 % in G250L2CT, respectively, of the eight decks' cracking torques. The enhancement was obvious, especially in double-layered reinforced solid deck G250L2ST (53.57 kN·m) and the most densely reinforced deck G100L2DDT (50.5 kN·m). It is worth mentioning that G100L2DDT achieved $T_{\varphi=0.07(\text{exp})}$ at least 26.8 % higher than any other decks except G250L2ST. This can be attributed to the diagonal bars, which increased the cracking torque weakened by the cutout, and the dense double-layered reinforcement mesh, which provided high post-cracking torsional rigidity. The decks with cutouts exhibited improved post-cracking torsional strength when reinforced with double-layered reinforcement arrangement, double diagonal bars, and a denser grid space. These enhancements resulted in a post-cracking torsional strength that was comparable to that of a double-layered reinforced solid deck. However, design engineers should consider the specific reinforcement details when evaluating the post-cracking torsional rigidity of GFRP-RC pontoon decks. The single layer reinforced decks G150L1DT, G150L1DDT, G150L1ST, and double layer reinforced decks G250L2CT, G250L2DT and G250L2DDT all failed due to cracking which was supported by crack propagation observation and the strain data analysis. Their actual post-cracking torsional strength is essentially the cracking torque. On the contrast, G100L2DDT and G250L2ST maintained narrow crack width and sound post-cracking torsional rigidity after cracking, so the post-cracking strength can be calculated based on the achieved twist angle, which is described latter in this study.

4.5. Prediction of cracking torque

The cracking torque equation introduced in ACI 318–14 [48] have been assessed as the most accurate prediction method for GFRP reinforced concrete beam and slabs tested in the previous studies [28,30]. The ACI 318–14 method is based on a thin-wall, hollow-space truss analogy and is expressed as:

$$T_{cr} = 0.33\sqrt{f_c} \left(\frac{A_{cp}^2}{P_{cp}} \right) \quad (1)$$

where A_{cp} is the area enclosed by the outside perimeter of the concrete cross section; and P_{cp} is the outsider perimeter of the concrete cross section.

Table 3 tabulated the estimated cracking torque $T_{cr(\text{pre})}$ with error in percentage. Note that the edge cutout without diagonal reinforcement was considered by reducing deck's effective width in the mid length of the deck from 1.5 m to 1.2 m as the cutout is 300 mm deep [30], and they resulted in 21.5 % less predicted cracking torque. The reduction is close to the difference between $T_{cr(\text{exp})}$ of G250L2CT and $T_{cr(\text{exp})}$ of G250L2ST, which was 17.9 %. In addition, the decks with diagonal bars

were considered to have same effective width as the solid decks since the experimental results indicate that the diagonal bars could bridge the shear crack in edge cutouts, resulting in higher torsional cracks. The prediction cracking torque of the other seven decks had a standard deviation of 3.8 kN·m compared to the experimental results. In conclusion, the ACI318–14 equation—when considering the effect of edge cutout and diagonal bars—provided good estimates of the tested decks' cracking torque.

4.6. Prediction for post-cracking torsional strength

Yang et al. [30] proposed a simple method to predict the post-cracking behavior of the GFRP-RC decks by considering pure torsion happened to the longitudinal bars. This method is formulated as:

$$T_{\varphi} = T_{cr} + (GJ)_{\text{post}} \times \varphi \quad (2)$$

$$(GJ)_{\text{post}} = \sum_{i=1}^n G_{\text{gfrp}} I_i = G_{\text{gfrp}} \sum_{i=1}^n I_i \quad (3)$$

where G_{gfrp} is the shear modulus of GFRP bars; φ is the achieved twist after cracking; I_i is each longitudinal bar's polar moment of inertia around the longitudinal axis going through the deck's cross section centroid; and n is the total number of longitudinal bars.

Table 3 listed the calculated results of the post-cracking torsional rigidity with error in percentage and torsional strength at 0.070 rad/m twist $T_{\varphi=0.07(\text{exp})}$. In general, the $GJ_{\text{post}(\text{pre})}$ is in the same magnitude level of the experimental post-cracking torsional rigidity. As G250L2ST and G100L2DDT had the strongest post-cracking torsional rigidity and did not present any signs of failure until the test was stopped due to reaching the maximum loading stroke, Eq. 2 is suitable for predicting $T_{\varphi=0.07(\text{pre})}$ of G250L2ST and G100L2DDT with a difference between the predicted and experimental results of less than 8 %. In contrast, the other six decks experienced failure controlled by wide cracks that occurred following the initial torsional crack, so the post-cracking torsional rigidity is essentially the predicted cracking torque.

5. Conclusion

The report presents the main experimental outcomes of pure torsion tests conducted on GFRP-RC pontoon decks with an edge cutout. The study investigated different GFRP bar arrangements, diagonal bars, and grid space. The test results were analyzed, and the following conclusions were drawn based on the analysis:

- The edge cutout induced concentrated stress leading to the decks failing just after the initial crack due to wide cracks or concrete crumbling. The double-layered reinforcement with diagonal bars and dense grid space, however, significantly enhanced the torsional capacity of the deck, which did not fail until the test was stopped due to reaching the maximum load stroke.
- The diagonal bars enhanced the pre-cracking torsional behavior while their influence on the torsional performance after cracking was negligible. Both single and double set of diagonal bars can improve the cracking performance by up to 17.9 %, but only when they were applied together with double layer reinforcement arrangement, the pre-cracking torsional rigidity can be enhanced by 26 %. That is contributed by that the diagonal bars close to the concrete surface bridged the crack openings and constrained the shear cracks from expanding.
- The double-layered reinforced decks strengthened the post-cracking torsional rigidity by up to 100 % when compared with decks reinforced with only single layer. That is because the double-layered reinforcement arrangement created a vertical distance from each bar to the cross-section centroid and resulted in a higher torsional constant J .

- Dense grid space improved the post-cracking torsional behavior and cracking control. This can be attributed to the larger number of continuous longitudinal bars that provided additional torsion resistance and kept the torsional crack from expanding.
- The densely reinforced deck with double diagonal bars achieved similar torsional performance as the double-layered reinforced solid deck did within the tested twist deformation. The expected ultimate torsional capacity of G100L2DDT was, however, lower than that the solid deck as the edge cutout induced a high level of concentrated stress that was not fully handled by the diagonal bar and denser reinforcement.
- The ACI 318-14 equation yielded an accurate prediction of deck cracking torque with a standard deviation of only 12 % when considering the diagonal bars can eliminate the influence from edge cutout. Meanwhile, a method to predict post-cracking behaviour including post-cracking torsional rigidity and failure by considering the reinforcement details was introduced based on the test results.

Further research is required to investigate the effect of other parameters in the torsional design of GFRP-RC planks. Considering the time cost and safety risk in the physical experiment, numerical modeling like FEA in Abaqus is a good option. Moreover, theoretical method to predict the ultimate torsional capacity for the GFRP-RC planks without enclosed shear reinforcement warrants further exploration as it can be a guide for practical design.

CRediT authorship contribution statement

Allan Manalo: Conceptualization, Funding acquisition, Methodology, Project administration, Resources, Supervision, Writing – review & editing. **Omar Saleh AlAjarmeh:** Conceptualization, Formal analysis, Investigation, Supervision, Visualization, Writing – review & editing. **Xian Yang:** Conceptualization, Data curation, Formal analysis, Investigation, Methodology, Validation, Writing – original draft. **Zahra Gharineiat:** Methodology, Supervision, Writing – review & editing. **Shahrad Ebrahimzadeh:** Formal analysis, Investigation, Validation, Writing – review & editing. **Charles-Dean Sorbello:** Conceptualization, Funding acquisition, Project administration, Resources, Supervision, Writing – review & editing. **Senarath Weerakoon:** Conceptualization, Funding acquisition, Project administration, Resources, Supervision, Writing – review & editing. **Brahim Benmokrane:** Project administration, Supervision, Writing – review & editing.

Declaration of Competing Interest

The authors would like to declare and confirm that there is no conflict of interest of this manuscript.

Acknowledgments

The authors express their gratitude to the following organizations for their financial support: the Queensland Department of Transport and Main Roads (DTMR), the Advance Queensland Industry Research Fellowship Program (AQIRF 119–2019RD2), and the Natural Science and Engineering Research Council (NSERC) of Canada. The authors also thank Sustainable Alliance Pty Ltd (Inconmat) for providing the GFRP reinforcement, and Jetty Specialist for fabricating the precast-concrete pontoon decks. Special thanks go to the technicians and students at the University of Southern Queensland for their assistance during plank manufacturing and testing.

References

- [1] Wu W, He X, Yang W, Alam MS, Wei B, He J. Degradation factors and microstructure degradation characteristics of B/GFRP bars in harsh environment: a review. *Constr Build Mater* 2023;366:130246.
- [2] Maranan G, Manalo A, Benmokrane B, Karunasena W, Mendis P. Evaluation of the flexural strength and serviceability of geopolymer concrete beams reinforced with glass-fibre-reinforced polymer (GFRP) bars. *Eng Struct* 2015;101:529–41.
- [3] Adam MA, Said M, Mahmoud AA, Shanour AS. Analytical and experimental flexural behavior of concrete beams reinforced with glass fiber reinforced polymers bars. *Constr Build Mater* 2015;84:354–66.
- [4] Manalo A, AlAjarmeh O, Cooper D, Sorbello C, Weerakoon S, Benmokrane B. Manufacturing and structural performance of glass-fiber-reinforced precast-concrete boat ramp planks. *Structures*. Elsevier; 2020.
- [5] Hassanpour S, Khaloo A, Aliasghar-Mamaghani M, Khaloo H. Effect of compressive glass fiber-reinforced polymer bars on flexural performance of reinforced concrete beams. *Acids Struct J* 2022;119(6):5–18.
- [6] Araba AM, Zinkaah OH, Alhawati M, Ashour A. Experimental tests of two span continuous concrete beams reinforced with hybrid GFRP-Steel bars. *Structures*. Elsevier; 2023.
- [7] Nguyen-Minh L, Rovňák M. Punching shear resistance of interior GFRP reinforced slab-column connections. *J Compos Constr* 2013;17(1):2–13.
- [8] Choi K-B, Choi W-C, Feo L, Jang S-J, Yun H-D. In-plane shear behavior of insulated precast concrete sandwich panels reinforced with corrugated GFRP shear connectors. *Compos Part B: Eng* 2015;79:419–29.
- [9] AlAjarmeh O, Manalo A, Benmokrane B, et al. Behavior of circular concrete columns reinforced with hollow composite sections and GFRP bars. *Mar Struct* 2020;72:102785.
- [10] Maranan G, Manalo A, Benmokrane B, Karunasena W, Mendis P. Behavior of concentrically loaded geopolymer-concrete circular columns reinforced longitudinally and transversely with GFRP bars. *Eng Struct* 2016;117:422–36.
- [11] Razaqpur A, Bencardino F, Rizzuti L, Spadea G. FRP reinforced/prestressed concrete members: a torsional design model. *Compos Part B: Eng* 2015;79:144–55.
- [12] CSA. Design and construction of building structures with fibre-reinforced polymers. CAN/CSA-S806-12. Canadian Standards Association; 2012.
- [13] ACI. Guide for the design and construction of structural concrete reinforced with fiber-reinforced polymer (FRP) Bar, (440. 1R-15). American Concrete Institute; 2015.
- [14] Association MC. GB 50608-2010 technical code for infrastructure application of FRP composites. Beijing, Chian: China Planning Press; 2010.
- [15] Wiater A, Siwowski T. Serviceability and ultimate behaviour of GFRP reinforced lightweight concrete slabs: experimental test versus code prediction. *Compos Struct* 2020;239:112020.
- [16] Hollaway L. The evolution of and the way forward for advanced polymer composites in the civil infrastructure. *Constr Build Mater* 2003;17(6-7):365–78.
- [17] Lv Q, Lu Y, Liu Y. Vibration serviceability of suspended floor: Full-scale experimental study and assessment. *Structures*. Elsevier; 2021.
- [18] Hsu TTC. Torsion of structural concrete - a summary on pure tension. *PCA Dev Dep Bull* 1968;18:165–78.
- [19] Hsu TTC. Torsion of structural concrete-behavior of reinforced concrete rectangular members. *Spec Publ* 1968;18:261–306.
- [20] Hsu TTC. *Torsion Reinf Concr* 1984.
- [21] Ibrahim MS, Gebreyouhannes E, Muhdin A, Gebre A. Effect of concrete cover on the pure torsional behavior of reinforced concrete beams. *Eng Struct* 2020;216:110790.
- [22] Chiu H-J, Fang I-K, Young W-T, Shiau J-K. Behavior of reinforced concrete beams with minimum torsional reinforcement. *Eng Struct* 2007;29(9):2193–205.
- [23] Ju H, Lee D, Kim JR, Kim KS. Maximum torsional reinforcement ratio of reinforced concrete beams. *Structures*. Elsevier; 2020.
- [24] Rahal KN. Torsional strength of normal and high strength reinforced concrete beams. *Eng Struct* 2013;56:2206–16.
- [25] Kim M-J, Kim H-G, Lee Y-J, Kim D-H, Lee J-Y, Kim K-H. Pure torsional behavior of RC beams in relation to the amount of torsional reinforcement and cross-sectional properties. *Constr Build Mater* 2020;260:119801.
- [26] Lopes S, Bernardo L. Twist behavior of high-strength concrete hollow beams—formation of plastic hinges along the length. *Eng Struct* 2009;31(1):138–49.
- [27] Joh C, Kwahk I, Lee J, Yang I-H, Kim B-S. Torsional behavior of high-strength concrete beams with minimum reinforcement ratio. *Adv Civ Eng* 2019;2019.
- [28] Mohamed HM, Benmokrane B. Reinforced concrete beams with and without FRP bar reinforcement under pure torsion. *J Bridge Eng* 2016;21(3):04015070.
- [29] Deifalla A, Hamed M, Saleh A, Ali T. Exploring GFRP bars as reinforcement for rectangular and L-shaped beams subjected to significant torsion: an experimental study. *Eng Struct* 2014;59:776–86.
- [30] Yang X, AlAjarmeh O, Manalo A, et al. Torsional behavior of GFRP-reinforced concrete pontoon decks with and without an edge cutout. *Mar Struct* 2023;88:103345.
- [31] Lopes AV, Lopes SM, do Carmo RN. Stiffness of reinforced concrete slabs subjected to torsion. *Mater Struct* 2014;47(1):227–38.
- [32] Mohamed HM, Benmokrane B. Torsion behavior of concrete beams reinforced with glass fiber-reinforced polymer bars and stirrups. *Acids Struct J* 2015;112(5):543.
- [33] DTMR. *Design Criteria for Floating Walkways and Pontoons*. Queensland Department of Transport and Main Roads 2015; Available from: <https://www.tmr.qld.gov.au/business-industry/Technical-standards-publications/Design-criteria-Marine>.
- [34] Enochsson O, Lundqvist J, Täljsten B, Rusinowski P, Olofsson T. CFRP strengthened openings in two-way concrete slabs—an experimental and numerical study. *Constr Build Mater* 2007;21(4):810–26.
- [35] Anil Ö, Kaya N, Arslan O. Strengthening of one way RC slab with opening using CFRP strips. *Constr Build Mater* 2013;48:883–93.
- [36] Floruț S-C, Sas G, Popescu C, Stoian V. Tests on reinforced concrete slabs with cut-out openings strengthened with fibre-reinforced polymers. *Compos Part B: Eng* 2014;66:484–93.

- [37] Hussein MJ, Jabir HA, Al-Gasham TS. Retrofitting of reinforced concrete flat slabs with cut-out edge opening. *Case Stud Constr Mater* 2021;14:e00537.
- [38] Arabasi S, El-Maaddawy T. Reinforcing of discontinuity regions in concrete deep beams with GFRP composite bars. *Compos Part C: Open Access* 2020;3:100064.
- [39] Smith ST, Kim S. Strengthening of one-way spanning RC slabs with cutouts using FRP composites. *Constr Build Mater* 2009;23(4):1578–90.
- [40] CSA. Specification for fibre reinforced polymers. CAN/CSA-S806-10. Canadian Standards Association; 2010.
- [41] Benmokrane B, Manalo A, Bouhet J-C, Mohamed K, Robert M. Effects of diameter on the durability of glass fiber–reinforced polymer bars conditioned in alkaline solution. *J Compos Constr* 2017;21(5):04017040.
- [42] DTMR, *Transport and Main Roads Specifications MRTS70 Concrete*. Transport and Main Roads Specifications 2018.
- [43] Basaran B, Kalkan I. Investigation on variables affecting bond strength between FRP reinforcing bar and concrete by modified hinged beam tests. *Compos Struct* 2020;242:112185.
- [44] ASTM. Standard test method for tensile properties of fiber reinforced polymer matrix composite bars. D7205-11. ASTM; 2011.
- [45] Derkowski W, Surma M. Torsion of precast hollow core slabs. *Czasopismo Techniczne*; 2015.
- [46] Marti P, Leesti P, Khalifa WU. Torsion tests on reinforced concrete slab elements. *J Struct Eng* 1987;113(5):994–1010.
- [47] Hadhood A, Gouda MG, Agamy MH, Mohamed HM, Sherif A. Torsion in concrete beams reinforced with GFRP spirals. *Eng Struct* 2020;206:110174.
- [48] ACI, *Building code requirements for structural concrete*. ACI 318–14 and commentary 2014.